UC Davis
UC Davis Previously Published Works

Title

Modeling groundwater contaminant transport in the presence of large heterogeneity: a case study comparing MT3D and RWhet

Permalink

https://escholarship.org/uc/item/7c3638xh

Journal

Hydrogeology Journal, 27(4)

ISSN

1431-2174

Authors

Guo, Zhilin
Fogg, Graham E
Brusseau, Mark L
et al.

Publication Date

2019-06-01

DOI

10.1007/s10040-019-01938-9

Peer reviewed

Modeling groundwater contaminant transport in the presence of large heterogeneity: A case study comparing MT3D and RWhet

Zhilin Guo[1,*], **Graham E. Fogg**[1], **Mark L. Brusseau**[2], **Eric M. LaBolle**[1], **Jose Lopez**[1]

[1]Land, Air, and Water Resources, University of California, Davis, 1 Shields Ave, Davis, CA, 95616

[2]Soil, Water and Environmental Science Department, University of Arizona, 429 Shantz Bldg., Tucson, AZ 85721

Abstract

A case study is presented that implements two numerical models for simulating a 30-year PAT operation conducted at a large contaminated site for which high-resolution data sets are available. A Markov chain based stochastic method is used to conditionally generate the realizations with random distribution of heterogeneity for the Tucson International Airport Area (TIAA) federal Superfund site. The fields were conditioned to data collected for 245 boreholes drilled at the site. Both MT3DMS and the advanced random walk particle method (RWhet) were used to simulate the PAT-based mass removal process. The results show that both MT3DMS and RWhet represent the measured data reasonably, with Root Mean Square Error (RMSE) less than 0.03. The use of fine grids and the total-variation-diminishing method (TVD) limited the effects of numerical dispersion for MT3DMS. However, the effects of numerical dispersion were observed when compared to the simulations produced with RWhet using a larger number of particles, which provided more accurate results with RMSE diminishing from 0.027 to 0.024 to 0.020 for simulations with 1, 20, and 50 particles. The computational time increased with more particles used in the model, but was still much less than the time required for MT3DMS, which is an advantage of RWhet. By showing the results using both methods, this study provides guidance for simulating long-term PAT systems. This work will lead to improve understanding of contaminant transport and plume persistence, and in turn will enhance site characterization and site management for contaminated sites with large plumes.

Keywords

Pump and treat; Mass transfer; Heterogeneity; Geostatistics

Introduction

Groundwater resources contaminated by a variety of organic and inorganic contaminants used in industrial, commercial, agriculture, and other applications continue to pose significant threats to human health and the environment. Examples of compounds of concern include chlorinated solvents (e.g., trichloroethene, tetrachloroethene, carbon tetrachloride),

*Corresponding author: Department of Land, Air, and Water Resources, University of California, Davis, CA 95616, United States. zlguo@ucdavis.edu (Zhilin Guo).

1,4-dioxane, methyl tertiary-butyl ether (MTBE), and perchlorate. The transport processes of these contaminants are highly impacted by the heterogeneity and anisotropy of alluvial subsurface environments (e.g., Fogg 1998; Liu and Ball 2002; Chapman and Parker 2005; Brusseau et al. 2007, 2011; Parker et al. 2008; Bianchi et al. 2011; Seyedabbasi et al. 2012; Dearden et al. 2013; Brusseau and Guo 2014; Matthieu et al. 2014; Guo and Brusseau 2017). Extensive dissolved-phase plumes typically form at sites contaminated by these contaminants, which has been reported in many previous studies (e.g., Tompson et al. 1998; Lien and Wilkin 2005; Parker et al. 2008; Brusseau et al. 2011; Bichet et al. 2016; Robertson et al. 2016). These large plumes are very expensive to contain or completely cleanup, and pose difficulties for site management and closure.

The heterogeneity of the subsurface is a primary factor responsible for hampering groundwater remediation. The interconnected high-permeability network can impact groundwater flow patterns and provide preferential pathways for a relatively rapid migration of contaminants (Silliman and Wright 1988; Desbarats 1990; Desbarats and Srivastava 1991; Moreno and Tsang 1994; Lee et al. 2000; LaBolle and Fogg 2001). The low-permeability zones tend to retard contaminant transport and temporarily store the mass due to minimum flow through these zones. Contaminant diffusion to or from fine-grained materials provides a sink or source, which poses challenges to contaminant remediation (Askari et al. 1996; Grathwohl 1998; Fogg et al. 2000; LaBolle and Fogg 2001; Brusseau et al. 2007 and 2011; Seyedabbasi et al. 2012; Brusseau and Guo 2014; Matthieu et al. 2014). Therefore, a groundwater model that represents highly heterogeneous geologic and hydrogeologic systems is needed for reliable characterization and prediction of the groundwater flow and quality response to the remediation. However, detailed information to describe heterogeneity and anisotropy for a regional scale field is difficult and costly to obtain due to spatial variability of the subsurface and the relative scarcity of data on media properties.

Geostatistical and stochastic methods have been developed using geostatistical parameters deduced from available data, which are collected from borehole logs, pumping tests, and other means, to delineate the spatial distribution of hydraulic conductivity that can be incorporated into flow and transport. Gaussian random field models that are based on the mean, variance, and correlation scale of the hydraulic conductivity have been commonly used and yield reasonable representations (e.g., Dagan 1989; Gelhar 1993; Zhang 2002). However, as geological and geophysical data of continuous nature may not conform to Gaussian models (Journel 1983), more geologically-based models (e.g., indicator methods) have been developed. These geostochastic approaches closely tie to geologic processes and the sedimentary architecture (e.g. Journel and Gomez-Hernandez 1993; Webb and Anderson 1996; Fogg et al. 1998; Fogg et al. 2000). Carle and Fogg and colleagues (Carle, 1996; Carle and Fogg, 1996, 1997; Carle et al., 1998) developed the transition probability Markov chain approach, which incorporates the indicator geostatistical method with the available site information relating to textural and depositional facies, to characterize and simulate the heterogeneity. In addition to accurate characterization of the aquifer heterogeneity, it is also critical to accurately simulate contaminant migration including the mass transfer into and out the fine materials that are dominated by diffusion. Labolle and Fogg (2001) demonstrated the important role of diffusion on low permeability zones and the impact on pump and treat (PAT) at alluvial sites.

Significant complexity is involved in simulating spatial hydraulic conductivity variability at large scales, especially when coupled with diffusive mass transfer processes in heterogeneous media. This, along with the cost of requisite field sampling, limits our ability to conduct high-resolution simulations for large-scale, long-term pump and treat (PAT) systems. However, such simulations can be implemented when appropriate resources are available (e.g., Zhang and Brusseau, 1999; LaBolle and Fogg 2001; Guo and Brusseau 2017).

MT3DMS (Zheng and Wang 1999) has been commonly used to solve solute transport for field-scale problems. In addition, the total-variation-diminishing method (TVD) has been used as the solver to minimize numerical dispersion and eliminate spurious oscillations while preserving sharp concentration fronts (Zheng and Bennet 2002). However, TVD schemes are not as effective compared with the random walk method (Labolle 2006), which can eliminate numerical dispersion. However, because of the numbers of particles needed to represent contaminants and the time step to solve the problem, the random walk method generally has larger memory requirements.

The objective of this work is to employ a geostochastic approach coupled with diffusive mass-transfer representation to simulate PAT operations for a heterogeneous field site for which high-resolution data sets are available. Both the MT3DMS and random walk methods are used to simulate transport. The differences between the results obtained from the two methods are compared and discussed.

2. Methods

2.1 Site description

The selected site is part of the Tucson International Airport Area (TIAA) federal Superfund site in southern Arizona. The site corresponds to a facility that was used in the past to clean and service aircraft. Vapor degreasers, decarbonizers, and parts-cleaning tanks were located in several small buildings at the site. During the 1940's to mid-1970's, unlined pits and other features were used for the disposal of organic solvents, and contaminants entered the subsurface by seepage. In responsible to the detection of trichloroethene (TCE) in groundwater, the TIAA site was placed on the National Priorities List in 1983. A large, multiple-source plume of TCE exists in the upper portion of the regional aquifer. Administratively, the TIAA site is separated into three major zones, the North, Central, and South sections. The current study site is located within the south section of the complex.

The groundwater plume at the study site is approximately 5.5 km long and 1.0 km wide (Fig. 1) that resides in a shallow saturated zone (Brusseau et al. 2013). Aqueous concentrations of TCE as high as thousands of ug/L have been reported for groundwater sampled from monitoring wells. The PAT system was initiated in 1987 with 24 extraction wells, 20 injection wells, ~50 monitoring wells, and a groundwater treatment facility (URS 2016). The system remains operational as of December 2018. Over 13000 kg of Volatile organic compounds (VOCs) have been removed and the concentration of TCE has been reduced to ~25 ug/L from 350 ug/L, which however is still higher than the Maximum Contaminant Level of 5 ug/L.

The plume is located within alluvial sediments along the western edge of the Tucson Basin (URS 2016). Multiple hydrogeologic units are defined at the site, the unsaturated zone, 0 to ~40 meters below ground surface (m bgs); a laterally discontinuous surficial aquifer located above a discontinuous laterally extensive clay or sandy clay unit; the upper zone (UZ) of the Upper regional aquifer, 40 to 50 m bgs; a confining unit, 50 to 60 m bgs; the lower zone (LZ) of the Upper regional aquifer, 60 to 70 m bgs; a confining unit 70 to 90 m bgs; and the Lower regional aquifer, 90 m bgs to an unknown depth (Hargis and Montgomery, Inc. 1982). The potentiometric surface of the shallow groundwater zone is 28~29 m below land surface (bls). The TCE contaminants reside primarily in the UZ, which consists of clay and silty clay units, sand, and/or gravel units. A discontinuous laterally extensive clay or sandy clay unit in the unsaturated zone overlies the upper aquifer, and it serves as a confining layer where it is present. The lower aquifer consists of clayey sand and sandy clay with sand and gravel lenses. Ground water is under confined conditions in the lower aquifer. Potentiometric head in the lower aquifer is 18 to 37 m lower than in the upper aquifer (Mock et al. 1985).

Based on pumping tests, hydraulic conductivities ranging from 4×10^{-5} to 3×10^{-4} m/s were measured for the gravel sub-unit, and values from 1×10^{-6} to 5×10^{-6} m/s were measured for the primary clay unit above the gravel sub-unit. Natural groundwater flow is from southeast to northwest with natural hydraulic gradients for the gravel sub-unit ranging historically between 5×10^{-3} and 1×10^{-2}.

2.2 Simulation of geologic heterogeneity

The FORTRAN program T-PROGS, which is based on transition probability–Markov chain random-field approach described by Carle and Fogg (1996), Carle (1997), and Carle and Fogg (1997), was used in this study to generate the heterogeneous domain. Transition probabilities are determined and used to conditionally simulate realizations of hydrostratigraphy for each depositional direction (strike, dip and vertical) and then generate a three-dimensional (3D) realizations of random fields using the Markov chain model [Carle and Fogg 1997; Carle 1996; Carle et al. 1998]. The transition probability, which reflects the spatial continuity and juxtapositional tendencies of the facies, is defined as a probability given that a facie j is present at a location x, another facies k occurs at location x+h:

$$t_{jk}(\mathbf{h}_\phi) = \Pr\left\{ k \quad occurs \quad at \quad \mathbf{x} + \mathbf{h}_\phi \middle| j \quad occurs \quad at \quad \mathbf{x} \right\} \tag{1}$$

where is x is a spatial location, $\mathbf{h}_\phi$ is the lag (separation vector) between two spatial locations in the ϕ direction, and j, k denote mutually exclusive categories such as geologic units or facies. The Markov chain model is then used to fit the measured transition probability values and conditionally generate realizations with stochastic distributions of hydrofacies. The hydrofacies categories are identified by interpretation of well logs collected from a field.

In this study, 245 geological borehole logs collected from the site [Zhang and Brusseau 1998] were interpreted and categorized into four hydrofacies, clay, silty sand, sand, and gravel, with the proportion of 42.4%, 17.7%, 19.6%, and 20.3% for each category. Vertical lengths were determined directly from the borehole logs whereas strike and dip lengths were estimated through geologic interpretation, which are summarized in Table 1 [Carle and Fogg

1997; Carle et al. 1998]. The clay facies were used as background and symmetrical distribution of facies in lateral direction were assumed. The Markov chain model was then developed by fitting to the measured transition probabilities between four hydrofacies (Figure 2). A grid of 250 (strike) × 250 (dip) × 70 (vertical) nodes with 20.0 m × 20.0 m × 0.5 m spacing was used for the Markov chain model. The top of the generated domain coincides with the water table at the site. An example of a realization of the K-field is shown in Figure 3. The connectivity was calculated, which indicates the extensive interconnection and full percolation in 3D for both gravel and sand.

2.2 Groundwater flow model

Groundwater flow was simulated using MODFLOW, a 3D numerical (finite-difference) groundwater flow model [McDonald and Harbaugh 1988; Harbaugh et al. 2000]. The aquifer domain was discretized with the same grid as the geostatistical model. General head boundaries were used along the northwest and southeast corners of the domain, with a natural gradient (0.007) inducing lateral groundwater flow from southeast to northwest and no-flow boundaries were defined parallel to the direction of flow. The no-flow boundaries were set far from the area of interest to minimize boundary effects.

Spatially variable hydraulic conductivities (K) and porosities are assigned to individual cells according to the categories of hydrofacies for the corresponding cells from the geostatistical realization (Table 1). K and porosities for each hydrofacies used in the model were determined according to information generated from geologic borehole-logs, pumping tests, and historic data collected for the Tucson International Airport Area Superfund site (Zhang and Brusseau 1999). The simulations were conducted from 1987 to 2013, with a total simulation time of 9855 days. A total of 27 stress periods and 324 time steps are used. Samples of extracted water were collected and analyzed approximately once per month. The pumping rates, recorded continuously and tabulated monthly throughout the course of operation, for each well were used as input.

2.3 Solute transport model

The 3D solute transport in transient groundwater flow systems is described by the partial differential equation in MT3DMS (Zheng and Wang 1999). A random–walk based method, RWhet, was developed to solve transport problems without causing numerical dispersion (Labolle 2006), which adds an additional term to manage the discontinuities of the standard advection–dispersion equation and can be written as (LaBolle et al. 1996; Labolle 2006):

$$\frac{\partial}{\partial t}[\theta(\mathbf{x},t)c(\mathbf{x},t)] = -\sum_i \frac{\partial}{\partial x_i}[v_i(\mathbf{x},t)\theta(\mathbf{x},t)c(\mathbf{x},t)] + \sum_{i,j}\frac{\partial}{\partial x_i}\left[\theta(\mathbf{x},t)D_{ij}(\mathbf{x},t)\frac{\partial c(\mathbf{x},t)}{\partial x_j}\right]$$
$$+ \sum_k Q_k(\mathbf{x},t)c_k(\mathbf{x},t)\delta_k(\mathbf{x}-\mathbf{x}_k) + \sum_n R_n \tag{2}$$
$$- s_{dd}$$

where θ (dimensionless) is the porosity of the subsurface medium; c (M/L^3) is the dissolved concentration; $x_{i,j}$ (L) is the distance along the respective Cartesian coordinate axis; D

(L^2/T) is the hydrodynamic dispersion coefficient tensor, v_i (L/T) is the seepage or linear pore water velocity; c_k [M/L3] is the aqueous phase concentration in the flux Q_k [L3/T] of water at x_k, δ is a Dirac function; $\sum r_n$ (M/L^3/T) is the chemical reaction term; s_{dd} represents the rate of loss or gain of aqueous mass to and from a second domain in a dual domain (mobile-immobile) regime, such as would occur through matrix diffusion to and from the matrix domain in a fracture-matrix regime. The concentration of an aqueous solute is represented by a finite system of N_p particles of mass $m_p(t)$ via (Tompson 1987; LaBolle et al. 1996):

$$R\Theta(\mathbf{x})c^s(\mathbf{x}, t) = \sum_{p \in N_p} m_p \zeta\left(\mathbf{x} - \mathbf{X}_p(t)\right) \tag{3}$$

where R is the retardation factor; $X_p(t)$ is the location of particle p at time t; ζ is an interpolation, or projection function (Bagtzoglou et al. 1992) to "smooth" the spatial distribution of concentration.

The parameters used in the model were determined based on the data measured in lab experiments for TCE or from site tests reported in Zhang and Brusseau, 1999. The aqueous diffusion coefficient was 7.6×10^{-5} m^2/d and longitudinal, transverse and vertical dispersivities of 5, 0.5, and 0.05 m were used, respectively. First order kinetics was used for sorption of TCE, with a distribution coefficient of 0.04 cm^3/g and mass transfer coefficient of 15 d^{-1}, based on measured data for sediments collected from the site (Zhang and Brusseau 1999). The initial plume was determined according to the TCE distribution in 1987 prior to the commencement of PAT operations and assumed a uniform distribution in the vertical direction, which is reasonable given that the contaminants have resided in the aquifer for several decades.

The simulated composite flux-averaged TCE concentrations for all pumping wells were computed and compared to the observed composite concentrations that were measured for the influent to the treatment plant. No parameter fitting was conducted to match the observed concentration data. The flux-averaged concentration for all extraction wells in the system is defined as

$$\bar{C}(t) = \frac{\sum C_i(t)q_i(t)}{\sum q_i(t)} \tag{5}$$

where C_i is the vertically averaged TCE concentration for well i; q_i is the pumping rate for well i.

3.   Results

3.1   Time continuous concentration change

The simulated hydrographs were compared to the corresponding ones plotted using measured data from monitor wells. By fitting the hydrographs, the hydraulic conductivity for each hydrofacie was also calibrated. The K values used in the simulations are listed in Table 1 and selected hydrographs are presented in Figure 4. Acceptable matches between the

simulated heads and measured data are obtained for the first 14 years of data. Starting from 2000 (year 15), the measured groundwater levels have risen due to the combination of (a) less use of the central Tucson well field as Tucson has switched to Central Arizona Project water, and (b) the startup in 2000 of the Pima Mine Road recharge facility that is ~20 km south of the TIAA site. In this study, we did not attempt to simulate the groundwater level changes caused by these two projects because after 14 years of operation of PAT, it is reasonable to assume that most mass left at the site resides in low permeability zones and that the post-year 14 changes to flow did not impact mass removal significantly.

Time-continuous measured and simulated composite concentrations of TCE entering the treatment plant are plotted in Figure 5. Both MT3DMS and RWhet provided reasonable simulations of the measured data, with Root Mean Square Error (RMSE) less than 0.03 and correlation coefficients higher than 0.9 (Table 2). Inspection of scatter plots show that the simulated concentrations match relatively well with the measured values (Figure 6). It is observed that the simulated concentrations for all cases exceed the measured values from years 2 to 9. This is notable because the simulations do not include the presence of NAPL in the source zones, which is known to be present. The larger simulated concentrations are a result of the assumption of constant initial TCE concentration along the vertical dimension, whereas field data indicate lower concentrations reside at greater depth.

It is notable that the results from RWhet with more particles (20 particles and 50 particles) converge on a more accurate solution compared to the 1-particle simulation, with the RMSE diminishing from 0.027 to 0.024 to 0.020 (Table 2). Differences are also observed in the scatter plots in Figure 6. The results are reasonable as more particles provide higher resolution output. In contrast, the MT3DMS simulation appears to be impacted to a degree by numerical dispersion that resulted in the differences between MT3DMS and RWhet. As observed from Figure 5, the peak concentration is lower with MT3DMS because of the more dispersed solution. This also reflects on the spatial concentration distribution, shown in Figure 7. It is apparent that the plume generated by MT3DMS (Fig. 7a) is more spread out with lower concentration edges than the plume from RWhet. At the meantime, the plume from MT3DMS has fewer regions with relatively high concentrations compared with the plume from RWhet due to numerical dispersion. Observing the plumes generated by RWhet with different particle resolutions, the plume generated using 1 particle per cell is noisier, whereas the plumes generated with more particles are smoother and start to converge.

As discussed above, with more particles, RWhet can provide more accurate results by eliminating the impact from numerical dispersion. This is an advantage of the RWhet model, in that resolution can be increased through the addition of more particles, subject of course to computational constraints. In this study, the results obtained from MT3DMS are not greatly different from the RWhet results largely due to the fine grid spaces and small time steps used in the model. However, the degree to which a particular MT3DMS solution to a complex problem is impacted by numerical dispersion cannot be quantified without RWHet or a similar solution that eliminates numerical dispersion. Another critical factor to consider when conducting numerical simulations is the computational cost. In this study, we used a machine comprising two 2.40 GHz processors, 16 cores, and 32 GB memory. The simulations required approximately 92 hours for MT3DMS; whereas the time cost for

RWhet with 1 particle, 20 particles, and 50 partilces were 45 min, 17 hours, and 49 hours respectively. This is another advantage of the RWhet model.

3.2 Comparison with previous modeling study

Zhang and Brusseau (1999) simulated PAT operations at the same site, in which the domain was divided into 3 layers unevenly in the vertical direction, with each layer varying from 4–7 m in thickness. This upper section of the UZ represented in the simulations encompasses the vast majority of the TCE contaminated portion of the aquifer. Scenarios were simulated with and without the presence of solvent mass (NAPL) in the identified source zones for the period 1987 to 1998. To produce a comparable simulation using the current modeling approach, a simulation was conducted with a 20-m thick domain that covers the same range of aquifer in the vertical direction as Zhang and Brusseau (1999).

The results of the additional simulation are presented in Figure 8. As expected, the elution curve produced from the current model resides below the curve produced in the previous study with the presence of NAPL, as the current model does not incorporate the presence of NAPL. Comparison of the elution curves in Figures 5 and 8 shows that the concentrations for the simulation with a 20-m thick domain are lower than those for the original (35-m thick domain) simulations. These results highlight the impact of the additional solute mass present in the thicker domain on the simulated elution curves.

The 20-m domain simulation exhibits higher concentrations and greater tailing after the initial startup period compared to the elution curve produced in the prior study for the simulation without NAPL. Both of these cases represent the impact of hydraulic-conductivity heterogeneity and well-field hydraulics on contaminant removal. The disparity between these two elution curves is partially due to the different initial mass inputs employed, as the domain thickness in the prior model varied versus the uniform 20-m thickness used in the current model. Another difference is the pumping setup in the two models, wherein in the current study, the well screen depths were determined according to the reported data, whereas in the prior model, pumping was assigned to all three vertical layers. The third difference is the approach used to represent and generate the hydraulic conductivity field. The approach used in the current study is anticipated to better approximate the interconnected flow paths present in such a heterogeneous system, as discussed previously. This higher resolution may result in the generation of greater simulated preferential flow behavior, as well as more storage of mass in low permeability zones. This, along with more input dissolved mass and increased resolution of the well-screen locations, likely resulted in a higher-concentration and greater-tailing elution curve compared to the prior study.

4. Summary

A case study was presented wherein two models were used to simulate PAT operations for a heterogeneous alluvium contamination site, the Tucson International Airport Area (TIAA) federal Superfund site, located in Tucson, AZ. A Markov chain based stochastic method was used to conditionally generate hydraulic conductivity heterogeneity. Both MT3DMS and the advanced random walk particle method (RWhet) were used to simulate the PAT system.

The simulated results are compared with long-term high-resolution field data. Simulations conducted using both RWhet and MT3DMS fit the measured field data in an acceptable error range with RMSE lower than 0.03. RWhet with more particles provides more accurate results, with lower RMSE and higher correlation coefficient compared with MT3DMS by eliminating impacts from numerical dispersion, which can also be observed from the plume map. The ability to increase resolution with additional particles is an advantage of the RWhet model. Even though the computational time for RWhet increased with more particles used, it was still much lower than that required for MT3DMS, which is another significant advantage.

Acknowledgement

Reference

Askari MDF, Maskarinec MP, Smith SM, Beam PM, Travis CG (1996) Effectiveness of purge-and-trap for measurement of volatile organic compound in aged soils. Anal. Chem 68, 3431–3433. [PubMed: 21619276]

Bagtzoglou AC, Dougherty DE (1992) Application of particle methods to reliable identification of groundwater pollution sources. Water Resour. Manage 6:15–23.

Bianchi M, Zheng C, Wilson C, Tick GR, Liu G, Gorelick SM (2011), Spatial connectivity in a highly heterogeneous aquifer: From cores to preferential flow paths, Water Resour. Res 47, W05524, doi: 10.1029/2009WR008966

Bichet V, Grisey E, Aleya L (2016) Spatial characterization of leachate plume using electrical resistivity tomography in a landfill composed of old and new cells (Belfort, France). Engineering Geology. 211: 61–73

Brusseau ML, Nelson NT, Zhang Z, Blue JE, Rohrer J, Allen T (2007) Source-Zone Characterization of a Chlorinated-Solvent Contaminated Superfund Site in Tucson, AZ. J. Contam. Hydrol 90: 21–40. [PubMed: 17049404]

Brusseau ML, Hatton J, DiGuiseppi W(2011) Assessing the impact of source-zone remediation efforts at the contaminant-plume scale through analysis of contaminant mass discharge, J. Contam. Hydrol 126: 130–139. [PubMed: 22115080]

Brusseau ML, Guo Z (2014) Assessing contaminant-removal conditions and plume persistence through analysis of data from long-term pump-and-treat operations, J. Contam. Hydrol 164: 16–24. [PubMed: 24914523]

Carle SF (1996) A transition probability-based approach to geostatistical characterization of hydrostratigraphic architecture: Ph. D. dissertation, University of California, Davis pp 248.

Carle SF, Fogg GE (1996), Transition probability-based indicator geostatistics, Math. Geol, 28(4): 453–477.

Carle SF (1997), Implementation schemes for avoiding artifact discontinuities in simulated annealing, Math. Geol 29 (2): 231–244.

Carle SF, Fogg GE (1997) Modeling spatial variability with one- and multi-dimensional continuous Markov chains, Math. Geol, 29(7): 891–917.

Carle SF, LaBolle EM, Weissmann GS, Brocklin Van D, Fogg GE (1998) Conditional simulation of hydrofacies architecture: A transition probability/Markov chain approach, in Hydrogeologic Models of Sedimentary Aquifers, Concepts Hydrogeol. Environ. Geol. Ser, vol. 1, edited by Fraser GS, and Davis JM. pp 147–170, Soc. of Sediment. Geol., Tulsa, Okla.

Chapman SW, Parker BL (2005) Plume persistence due to aquitard back diffusion following dense nonaqueous phase liquid source removal or isolation, Water Resour. Res 41, W12411.

Dagan G (1989) Flow and Transport in Porous Formations, Springer-Verlag, Berlin, Heidelberg pp 465.

Dearden RA, Noy DJ, Lelliott MR, Wilson R, Wealthall GP (2013) Release of contaminants from a heterogeneously fractured low permeability unit underlying a DNAPL source zone, J. Contam. Hydrol 153: 141–155. [PubMed: 24119249]

Desbarats AJ (1990) Macrodispersion in sand-shale sequences, Water Resour. Res 26: 153–163, doi: 10.1029/WR026i001p00153.

Desbarats AJ, and Srivastava RM (1991), Geostatistical characteriza-tion of groundwater flow parameters in a simulated aquifer, WaterResour. Res, 27, 687–698, doi:10.1029/90WR02705.

Fogg GE, LaBolle LR, Weissmann GS (1998) Groundwater vulnerability assessment: Hydrogeologic perspective and example from Salinas Valley, California, in Assessment of Non-point Source Pollution in the Vadose Zone,Geophys Monogr. Ser, vol. 108, edited by Corwin DL, Loague K, and Ellsworth TR, pp. 45–61, AGU, Washington, D. C.

Fogg GE, Carle SF, Green C (2000). Connected-network paradigm for the alluvial aquifer system In: Zhang D, Winter CL (Eds.), Theory, Modeling, and Field Investigation in Hydrogeology: A Special Volume in Honor of Shlomo P. Neuman's 60th Birthday, Boulder, Colorado Geologic. Soc. Am. (Special Paper) 348, 25–42.

Gelhar LW (1993) Stochastic Subsurface Hydrology, Prentice Hall, New Jersey.

Grathwohl P (1998) Diffusion in Natural Porous Media: Contaminant Transport, Sorption/Desorption and Dissolution Kinetics, Kluwer Academic Publishers, Norwell, Massachusetts.

Guo Z, Brusseau ML (2017) The impact of well-field configuration and permeability heterogeneity on contaminant mass removal and plume persistence, J. Hazard. Mater 333: 109–115. [PubMed: 28342351]

Harbaugh AW, Banta ER, Hill MC, McDonald MG (2000) MODFLOW-2000, The U.S. Geological Survey modular ground-water model-user guide to modularization concepts and the ground-water flow process, U.S. Geological Survey Open-File Report.

Hargis and Montgomery, Inc. (1982) Phase II investigation of subsurface conditions in the vicinity of abandoned waste disposal sites, Hughes Aircraft Company manufacturing facility Tucson, Arizona, Vol. I.

Journel AG (1983) Non-parametric estimation of spatial distributions. Math. Geol 15: 445–468.

Journel AG, Gomez-Hernandez JJ (1993) Stochastic imaging of the Wilmington clastic sequence. SPE Formation Eval. 33–40.

LaBolle EM, Fogg GE, Tompson AFB (1996) Random-walk simulation of transport in heterogeneous porous media: local mass-conservation problem and implementation methods. Water Resour. Res 32 (3): 583–593.

LaBolle EM, Fogg GE (2001) Role of molecular diffusion in contaminant migration and recovery in an alluvial aquifer system, Transp. Porous Media, 42: 155–179.

LaBolle EM (2006) RWHet: Random Walk Particle Model for Simulating Transport in Heterogeneous Permeable Media, Version 3.2, User's Manual and Program Documentation.

Lee CH, Hsu CC, Lin TK (2000) Study of multiple-layers groundwater resources management in Cho-Shui alluvial fan (in Chinese). J Taiwan Water Conserv 48:41–52

Lien HL, Wilkin RT (2005) High-level arsenite removal from groundwater by zero-valent iron. Chemosphere, 59(33): 377–386. [PubMed: 15763090]

Liu CX, Ball WP (2002) Back diffusion of chlorinated solvent contaminants from a natural aquitard to a remediated aquifer under well-controlled field conditions: Predictions and measurements, Ground Water, 40: 220–220.

Matthieu DE III, Brusseau ML, Guo Z, Plaschke M, Carroll KC, Brinker F (2014) Persistence of a groundwater contaminant plume after hydraulic source containment at a chlorinated-solvent contaminated site, Groundwater Monitoring and Remediation, 34: 23–32.

McDonald MG, Harbaugh AW (1998) A modular three-dimensional finite-difference ground-water flow model. U.S. Geological Survey Techniques of Water-Resources Investigations. Chapter A1, pp 586.

Moreno L, Tsang CF (1994) Flow channeling in strongly heteroge-neous porous media—a numerical study, Water Resour. Res 30: 1421–1430, doi:10.1029/93WR02978.

NRC (2013), Alternatives for managing the nation's complex contaminated groundwater sites. Washington, D.C.

Parker BL, Chapman SW, Guilbeault MA (2008) Plume persistence caused by back diffusion from thin clay layers in a sand aquifer following TCE source-zone hydraulic isolation, J. Contam. Hydrol 102: 86–104. [PubMed: 18775583]

Robertson WD, Van Stempvoort DR, Roy JW, Brown SJ, Spoelstra J, Schiff SL, Rudolph DR, Danielescu S, and Graham G (2016) Use of an artificial sweetener to identify sources of groundwaternitrate contamination. Groundwater. 54:579–587

Seyedabbasi MA, Newell JC, Adamson DT, Sale TC (2012) Relative contribution of DNAPL dissolution and matrix diffusion to the long-term persistence of chlorinated solvent source zones, J. Contam. Hydrol 134: 69–81. [PubMed: 22591740]

Silliman SE, Wright AL (1988) Stochastic analysis of paths of high hydraulic conductivity in porous media. Water Resour. Res, 24: 1901–1910.

Tompson AFB, Vomoris EG, Gelhar LW (1987) Numerical simulation of solute transport in randomly heterogeneous porous media: motivation, model development, and application. Rep. UCID-21281, Lawrence Livermore Natl. Lab., Livermore, CA

Tompson AFB, Carle SF, Rosenberg ND, Maxwell RM (1999) Analysis of groundwater migration from artificial recharge in a large urban aquifer: A simulation perspective, Water Resour. Res 35(10): 2981–2998.

URS (2016) Final-Annual Optimized Exit Strategy, Performance Metric Report, July 2014 to June 2015, OT012 – South of Los Reales Road, Regional Groundwater Plume, Air Force Plant 44, Tucson, Arizona.

Webb EK, Anderson MP (1996) Simulation of preferential flow in three dimensional, heterogeneous conductivity fields with realistic internal architecture. Water Resour. Res 32(3):533–45

Zhang Z, Brusseau ML (1998) Characterizing three-dimensional hydraulic conductivity distributions using qualitative and quantitative geologic borehole data: Application to a field site, Groundwater, 36: 671–678.

Zhang Z, Brusseau ML (1999) Nonideal transport of reactive solutes in Heterogeneous porous media 5. Simulating regional-scale behavior of a trichloroethene plume during pump-and-treat remediation. Water Resour. Res 35(10): 2921–2935.

Zhang D (2002) Stochastic Methods for Flow in Porous Media: Coping With Uncertainties, Academic San Diego, Calif pp 350.

Zheng C, Wang P (1999) MT3DMS: A Modular Three-Dimensional Multispecies Transport Model for Simulation of Advection, Dispersion, and Chemical Reactions of Contaminants in Groundwater Systems; Documentation and User's Guide. Contract Report SERDP-99–1.Vicksburg, Mississippi: U.S. Army Engineer Research and Development Center.

Zheng C, Bennett GD (2002) Applied contaminant transport modeling, Wiley Interscience New York.
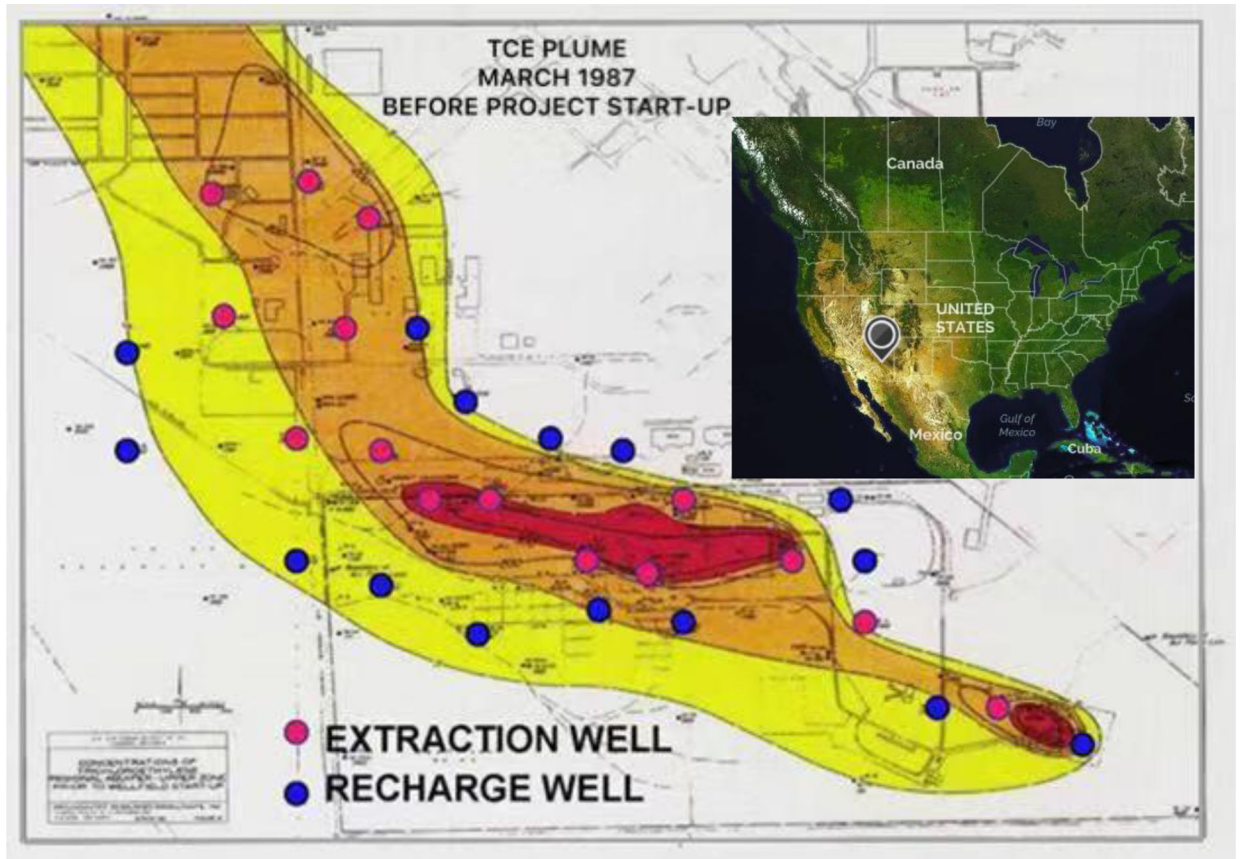
Figure 1.
Groundwater contaminant plume in 1987 before pumping was initiated. The locations of extraction and injection wells for the PAT systems are presented.
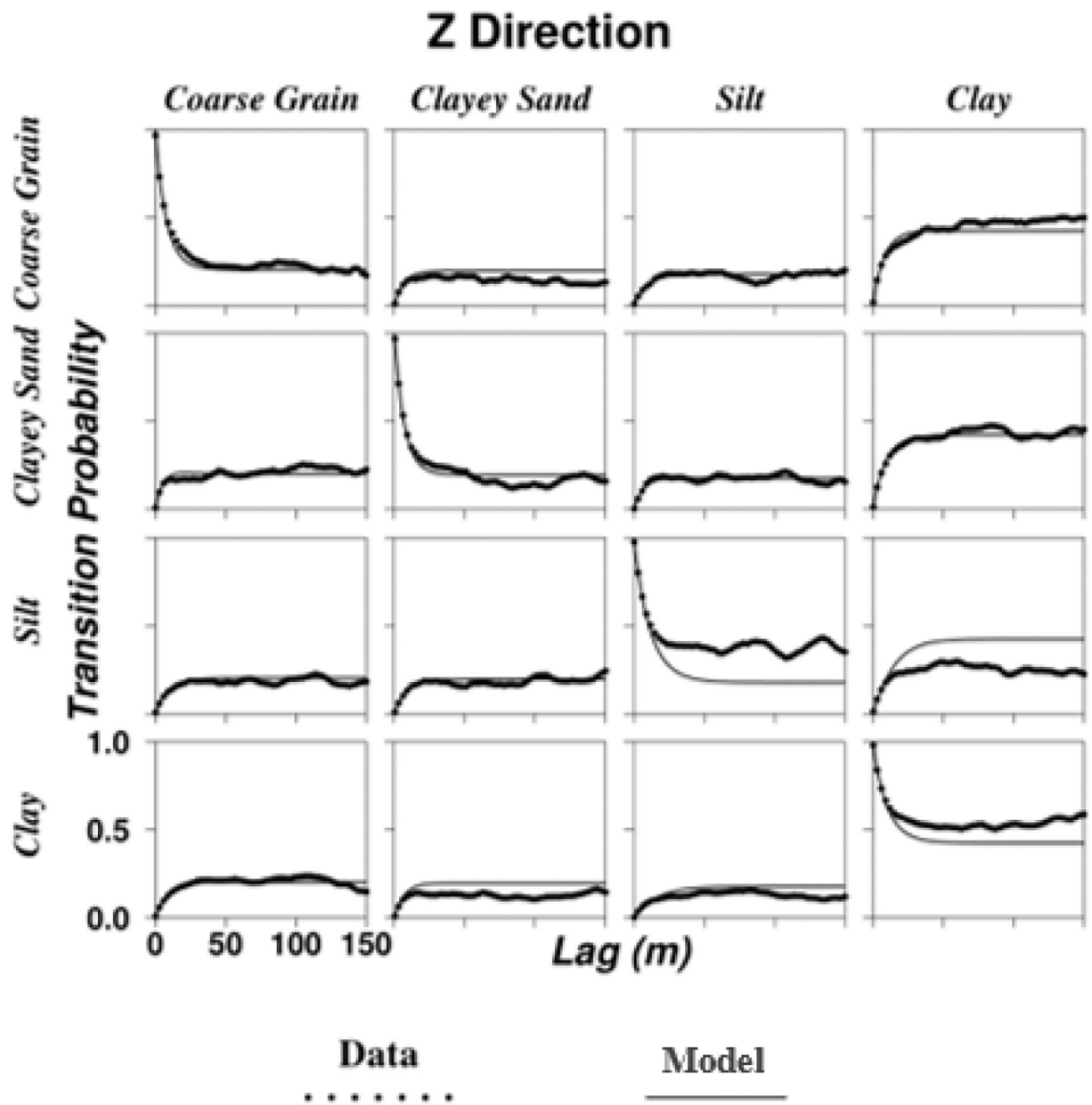
Figure 2.
Matrix of vertical (z)-direction transition probabilities showing core data measurements (dots) and the Markov chain model (solid lines). The diagonal elements represent auto-transition probabilities within a category, and the off-diagonal elements represent cross-transition probabilities between categories.
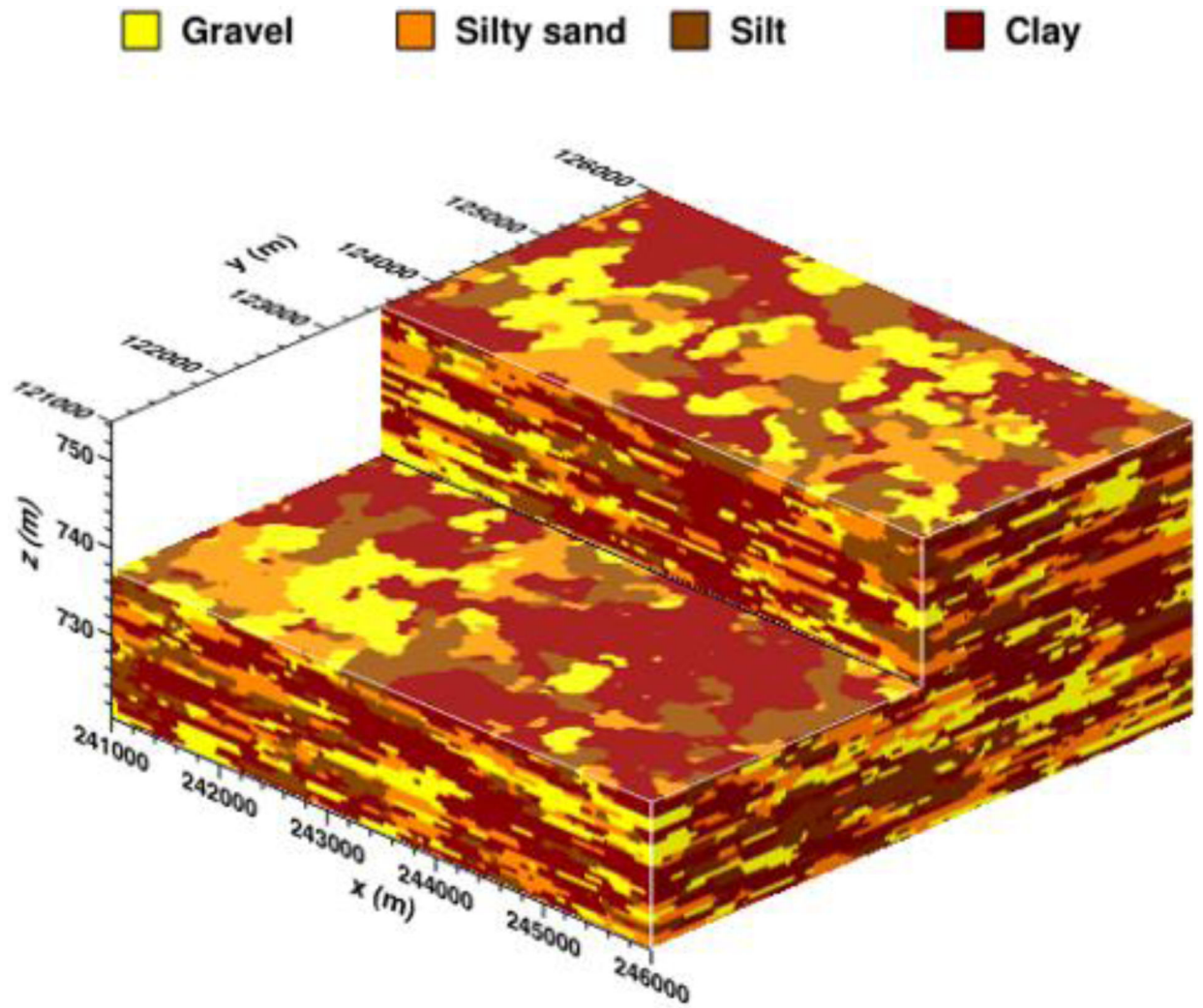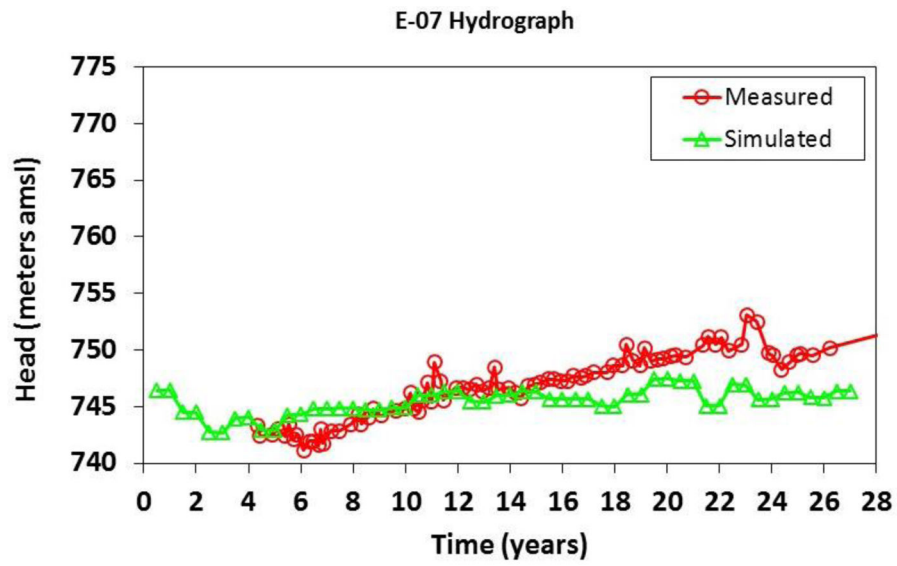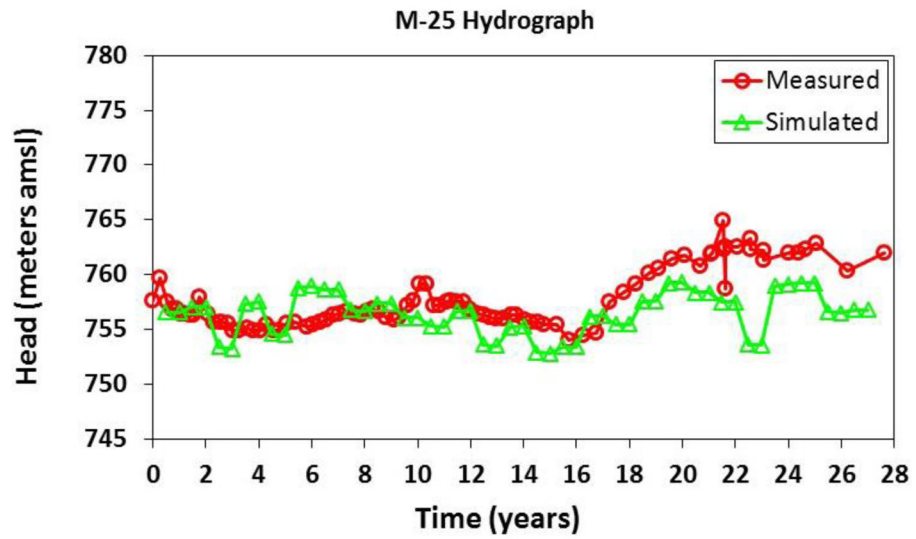
Figure 3.
A realization of the generated heterogeneous domain.

(a)

(b)

Figure 4.
Hydrographs for two wells, E-07 (located downgradient section of the plume) and M-25 (located in the middle section of the plume).
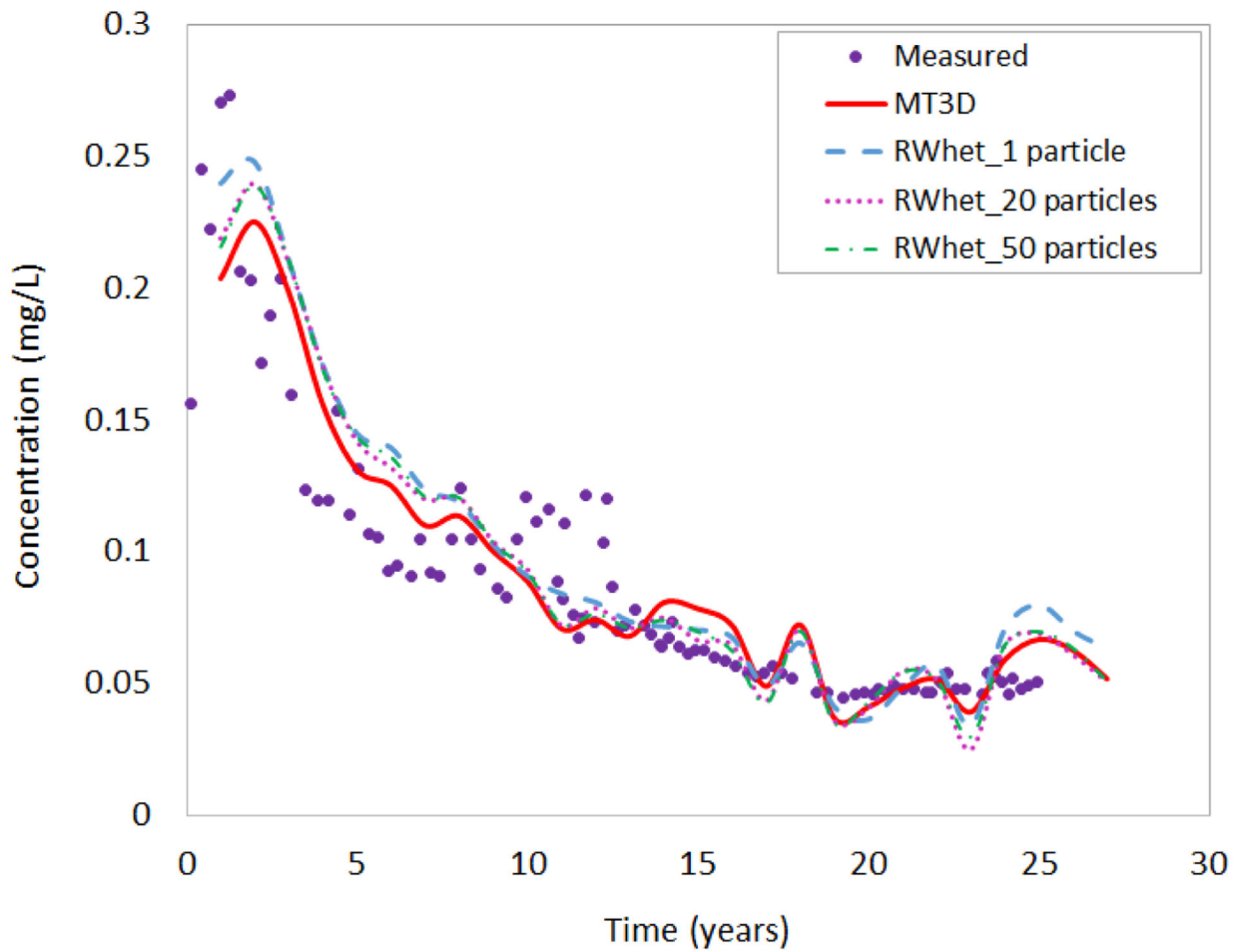
Figure 5.
Time continuous TCE concentrations. The measured data were collected from the influent to the treatment plant, thus representing a composite concentration for the entire PAT well field. Simulated results from MT3DMS and RWhet are the composited flux-averaged concentration calculated by the concentration data collected from each extraction well.
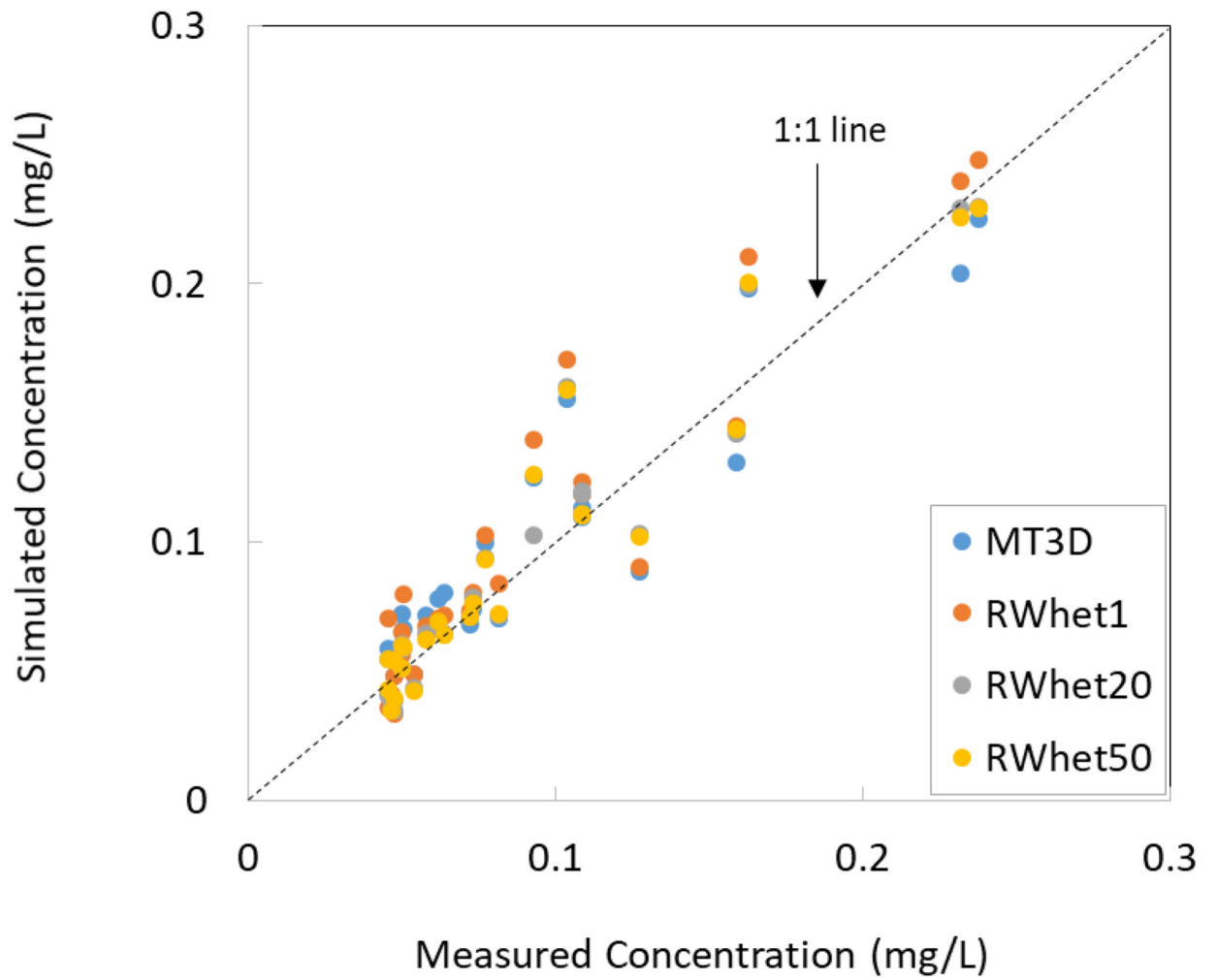
Figure. 6.
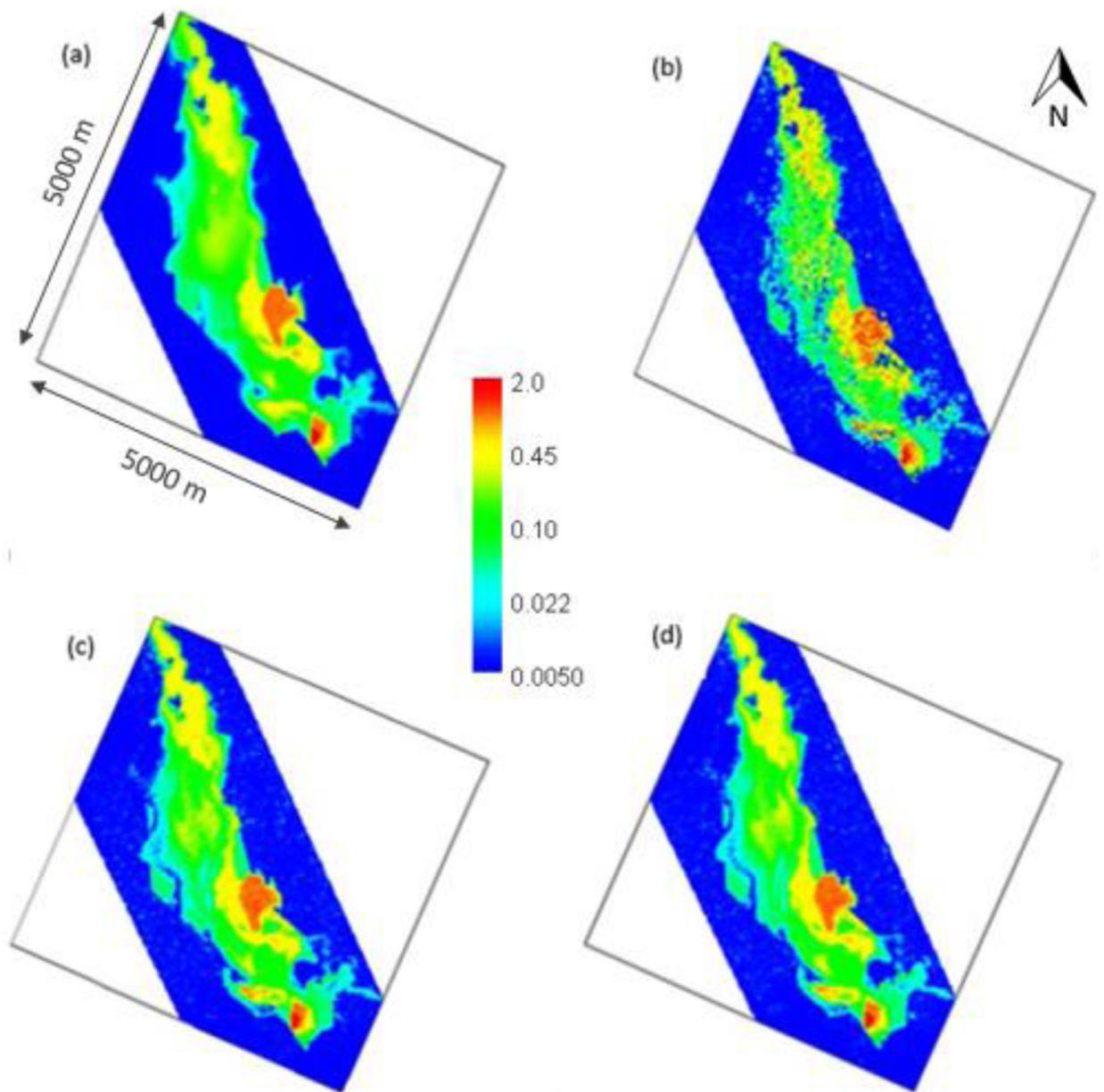Simulated concentrations from MT3DMS and RWhet versus the measured values.

Figure 7.
The simulated TCE plume from (a) MT3DMS, (b) RWhet with 1 particle per cell, (c) RWhet with 20 particles per cell, (d) RWhet with 50 particles per cell.
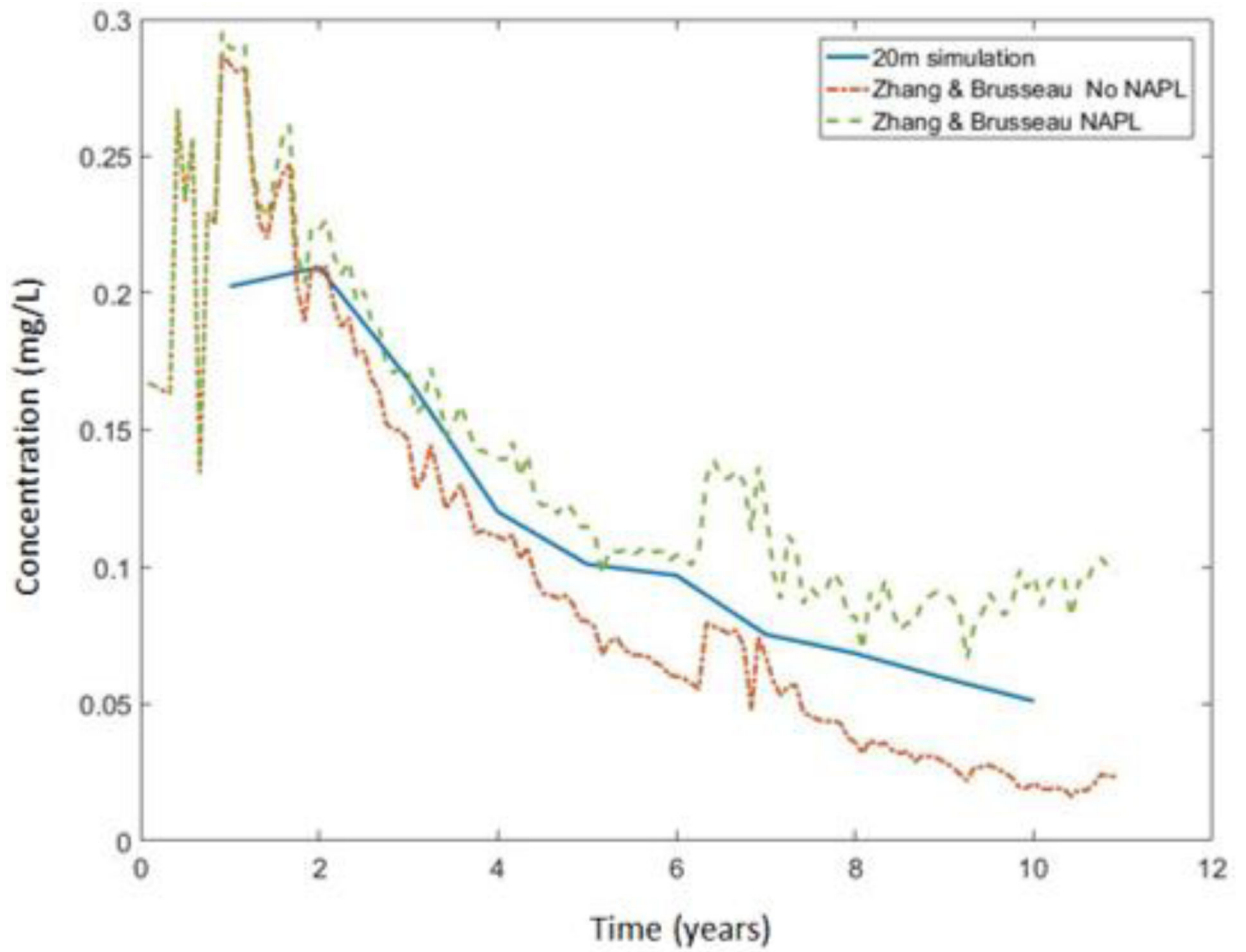
Figure 8.
Comparison of TCE elution curves simulated in this work (20 m simulation) with a previous study conducted by Zhang and Brusseau, 1999.

Table 1

Hydraulic conductivity, K, and porosity of the four hydrofacies for the heterogeneous simulations.

Hydrofacies	K, m/d	Porosity	Direction and mean length		
			Strike (m)	Dip (m)	Vertical (m)
Coarse Grain	124	0.2	360	500	9.6
Sand	45	0.2	200	265	8.6
Silt	3	0.2	380	350	13.8
Clay	0.00013	0.3	880	700	16.9

Table 2

RMSE and correlations between simulations and measured data.

	RMSE	Correlation
MT3D	0.027	0.926
RWhet (1particle)	0.027	0.925
RWhet (20particles)	0.024	0.930
RWhet (50particles)	0.020	0.932